http://dx.doi.org/10.4071/isom-2015-WA53
Authors' Postprint:

Thermal Aging Behavior of Fine Pitch Palladium Coated Silver (PCS) Ball Bonds on Al Metallization

Di Erick Xu[1], Jimy Gomes[1], Michael Mayer[1], Rob Lyn[2], John Persic[2]
1. Microjoining Laboratory, Centre for Advanced Materials Joining, Department of Mechanical and Mechatronics Engineering, University of Waterloo, Waterloo, Ontario, Canada N2L3G1
2. Microbonds Inc., 151 Amber St, Unit 12 Markham ON L3R 3B3 Canada
Keywords: Fine pitch, Pd coated Ag wire bond, high temperature storage test, intermetallic compound.

Abstract

The high price of Au has motivated many to look for alternative bonding wire materials in the field of microelectronics packaging. In the present study, the reliability performance of palladium coated silver (PCS) wire in high temperature storage test (HTST) is carried out using 18 µm diameter fine pitch PCS wire. Fine pitch ball bonds are made on Al metallization, with bonded ball diameter (BBD) of 32 ± 0.5 µm and ball height (BH) of 8 ± 0.5 µm. The aging temperature used in HTST is 170 °C and both shear and pull test are used to evaluate the aged ball bonds at regular time intervals. The shear force increases from 9.9 gf at 96 h to 12.5 gf at 192 h, and remains almost constant until 1344 h, and starts dropping gradually until 10.9 gf at 1848 h. The pad lift percentage recorded in pull test gradually drops from 90 % at 96 h to 20 % at 1008 h, and increases to 90 % at 1848 h. The chip side fractography after shear test indicates that the main failure modes are through pad at 96 h, through ball bond at 504 h, and half of both at 168 h, respectively. Cross-sectional images show that the thickness of the intermetallic compound (IMC) layer growth follows parabolic relationship and the rate constant is 0.10 ± 0.02 µm/h$^{1/2}$. Gaps are observed along the periphery of the ball bond interface where no IMC is observed. The IMCs are located at the center of the ball bond interface, and the width is 16.0-19.3 µm at 96 h and 17.2-22.7 µm at 1344 h, respectively.

Keywords: Fine pitch, Pd coated Ag wire bond, high temperature storage test, intermetallic compound.

1. Introduction

Wire bonding is the most widely used in chip-scale interconnection technology in microelectronics packaging. Au ball-wedge bond is the most widely used in wire bonding industry due to its high bondability and acceptable reliability. However in some cases, alternative wires are preferred due to the high cost of Au.

Cu wire costs less than Au, but readily oxidizes in air and requires shielding gas in free air ball (FAB) formation. Moreover, the high hardness of Cu FAB causes more Al pad splashing and higher chance of cratering.

With its lower cost than Au as well as its higher resistance to oxidation and lower hardness than Cu, the poor reliability of Ag with Al metallization can prevent Ag from being a suitable alternative to Au. Recent studies have found that alloying Ag with Pd and/or Au can result in improved ball bond reliability on Al metallization. The presence of Pd at the bond interface proves to be beneficial for reliability [1-6].

Rui Guo et al. [1] studied ball bond interface of Ag–8Au–3Pd wire and Al metallization. Two intermetallic regions at the interface were identified as $AuAl_2$ + $(Au, Ag)_4Al$ and Ag_2Al, respectively. The enthalpy of formation of Au aluminides is about one order of magnitude lower than Ag aluminides, which means that Au aluminides are easier to form than Ag aluminides [1]. In a thermal aging test of a ball bond on Al pad, the IMC layer grows faster by about 3 times for a pure Au than for a Au-30Ag alloy [2]. The main IMC relevant failure of Au ball bond on Al is commonly due to Kirkendall voids or the brittleness of the Au-Al IMCs [3].

Jong-Soo Cho et al. [4] showed that the higher content of Pd in Ag wire, the slower the ball bond interface degrades on Al metallization in a pressure cooker test. In a 12 h pressure cooker test, a crack as well as an alumina layer are observed between Ag and Al, without any observation of Ag-Al IMCs. Such crack and alumina layer are not observed with Ag-3Pd wire with the same test condition [4]. Yi-Wei Tseng et al. [5] have shown that wire annealing at 275 °C prior to bonding helps reduce the IMC growth rate at the ball bond interface of Ag-2Pd on Al pad.

Although Ag alloy wire has better reliability than Ag wire, it has substantially lower electrical conductivity than pure Ag, and is more expensive to produce. Moreover, the Ag alloy wire FAB can be defective when the ball size is too small. For example, for a 95 % Ag alloy

International Symposium on Microelectronics: FALL 2015, Vol. 2015, No. 1, pp. 000298-000304
http://www.imapsource.org/doi/abs/10.4071/isom-2015-WA53
http://dx.doi.org/10.4071/isom-2015-WA53
Authors' Postprint:

wire, the FAB is prone to voids and nodes when its size is less than 31 µm [6], which limits its application in a fine pitch process.

An alternative way to introduce Pd into the Ag-Al bond interface is to use Pd coated Ag (PCS) wire [7] which uses less Pd than alloyed wire and has the same electrical conductivity as pure Ag. PCS wire forms high quality FABs in air without any shielding gas [7]. For Pd coated Cu wire, Pd can be more concentrated on the FAB surface when the spark hits the wire tip from below and not from one side [8]. Similarly, PCS is expected to direct the spark to the wire tip from below due to arc constriction by the Pd layer [9], resulting in more Pd at the FAB surface and subsequently at the ball bond interface.

While the reliability improvement due to the alloying of Ag wire bonds has been investigated in some detail, the knowledge about the reliability of PCS wire is limited. In this study we investigate the reliability of PCS wire under high temperature storage (HTS).

2. Experimental

The wire used in this study is an 18 µm direct Pd coated Ag (PCS) wire from Microbonds Inc., Markham, Canada. The coating thickness is measured to be 90-120 nm with a field emission scanning electron microscope (FESEM). Accordingly, the calculated overall content of Pd is 1.13-1.51 wt.%, and is 62-72 % less than the Pd content in a Ag-4Pd wire. A comparison of Pd content in PCS wire and AgPd alloy wire is calculated and shown in Figs. 1a and b. The thickness of the Al metallization is 1.4-1.5 µm.

The ball bonds are optimized with the wire bonder and method described in [10]. The target ball bond geometry is shown in Fig. 2. A cross-section of the target ball diameter at capillary imprint (BDC) and bonded ball height (BH) are 32 ± 0.5 µm and 8 ± 0.5 µm. The parameters for electrode flame-off (EFO) and ball bonds are shown in Table 1. The capillary is a commercially available slim bottle neck capillary with a hole diameter of 23 µm and a chamfer diameter of 27 µm. The chamfer angle is 90° and the face angle is 8°. An illustration of the cross-section of the capillary tip is shown in Fig. 3. A scanning electron microscope (SEM) image of a bonded ball is shown in Fig. 4. The wedge bonds are made on gold metallization on a polymer substrate and showed no Non-Stick-on-Lead or Short-Tail, and no peeling [11].

The wire bonds are aged in air at 170 °C. The samples are heated and cooled inside the oven with a nominal

Table 1: The Electrical flame-off (EFO) parameters and ball bond parameters

	Parameter	Value
EFO	EFO current [mA]	60
	EFO time [ms]	0.096
	Electrode-wire distance [µm]	100
	Tail length [µm]	400
Ball bond	Bond force [mN]	56
	Bond time [ms]	20
	Impact force [mN]	164
	Ultrasonic Power [%]	25
	Temperature [°C]	200

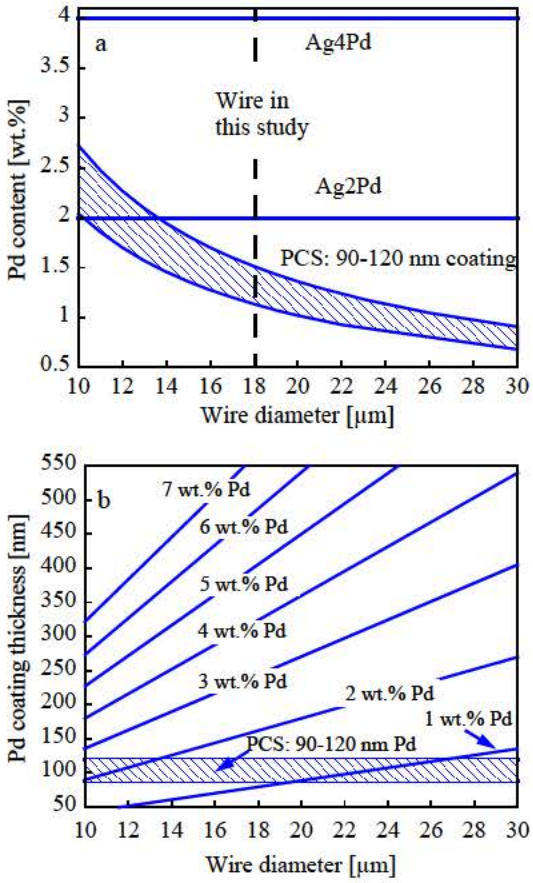

Figure 1. The calculated (a) Pd content in different wires, and (b) Pd coating thickness with different amount of Pd, for wire diameters of 10-30 µm.

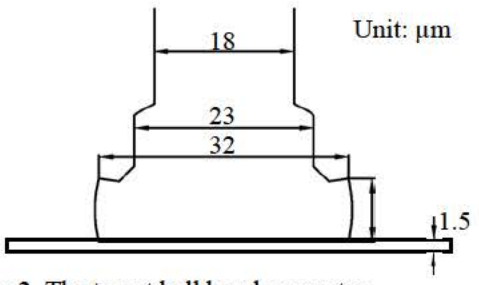

Figure 2. The target ball bond geometry.

International Symposium on Microelectronics: FALL 2015, Vol. 2015, No. 1, pp. 000298-000304
http://www.imapsource.org/doi/abs/10.4071/isom-2015-WA53
http://dx.doi.org/10.4071/isom-2015-WA53
Authors' Postprint:

heating and cooling rate of 40 °C/min. Both shear test and pull test are used to evaluate the ball bonds after various times of aging. The shear height is 3 µm and the shear test speed is 30 µm/s. The pull hook is placed very close to the ball bond. The pull test speed is 50 µm/s. Too fast test speed can result in higher forces because of the strain rate effect. Fractographies are taken with SEM and optical microscope. For cross-sectioning study, the samples are mounted with Epofix and ground with sand paper. The final surface finish is done by Ar ion milling.

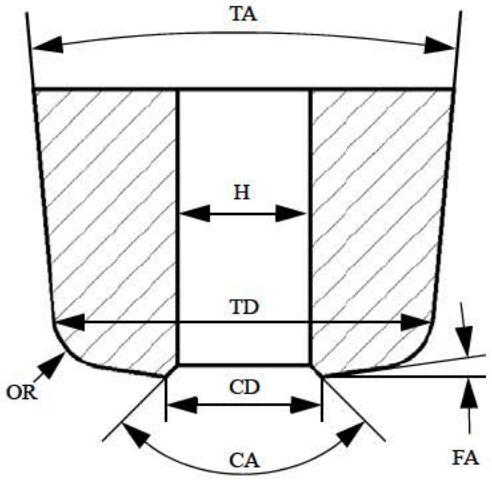

Figure 3. The illustration of a cross-section of the capillary used in this study, where TA = 10°, H = 23 µm, TD = 66 µm, CD = 27 µm, CA = 90°, OR = 10 µm, and FA = 8°.

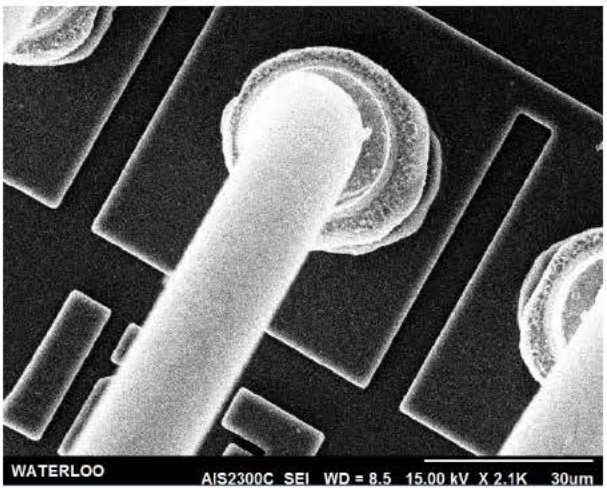

Figure 4. SEM image of a bonded ball using 18 µm PCS wire on Al metallization.

3. Results

3.1 Shear and pull test

The shear test results are shown in Fig. 5 and the pull test results are shown in Figs. 6a-b. The sample size is 10 for all the test groups. The maximum whisker length in the box plots is defined as 1.5 times the difference between first and third quartiles. The shear strength values are calculated with:

$$SS = \frac{SF}{\pi\left(\frac{BDC}{2}\right)^2} \quad (1)$$

where SF is the shear force, and BDC = 32 µm.

The ball bond shear force results are shown in Fig. 5 and increases from an average of 9.9 gf at 96 h to an average of 12.5 gf at 192 h. The average shear force values from the six measurement between 192 h and 1008 h range from 12.0 to 13.2 gf. The change in pull force along the aging test is not as obvious as the change of shear force. The pull force rises to a maximum of 6 gf after 600 h aging, and these samples all broke at the heat affected zone (HAZ). Most of the pad lift failures coincide with pull force values lower than 5.6 gf, indicated by the dashed line in Fig. 6a. HAZ breaking and pad lift are the only observed failure modes in the pull test. A typical chip side fractography after pad lift is shown in the inset of Fig. 6b. The pad lift percentage generally decreases from 90 % at 96 h to 20 % at 1008 h, and increases to 90 % at 1848 h, as shown in Fig. 6b.

Micrographs of typical fractographies on the chip side after ball bond shear test are shown in Figs. 7a and b (SEM) and Figs. 7c and d (optical). Pad shear and ball shear are the only observed failure modes. The failure mode is pad shear for all the 10 samples at 96 h. The

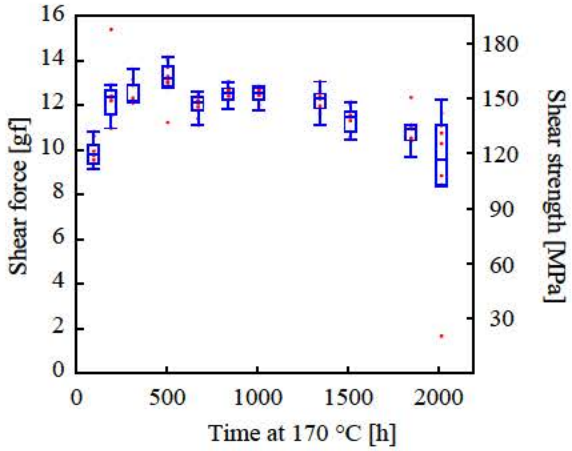

Figure 5. Ball bond shear force from 96 h to 2016 h aging in 170 °C.

International Symposium on Microelectronics: FALL 2015, Vol. 2015, No. 1, pp. 000298-000304
http://www.imapsource.org/doi/abs/10.4071/isom-2015-WA53
http://dx.doi.org/10.4071/isom-2015-WA53
Authors' Postprint:

number of samples with ball shear failure mode are 5/10 and 9/10 at 168 h and 504 h, respectively. The main failure mode changing from pad shear to ball shear indicates the formation of IMCs with strong adhesion.

3.2 IMC thickness

Cross-sections are made at 96 h, 504 h, and 1344 h. The optical images of typical samples are shown in Figs. 8a-c, respectively. The thickness of the IMC layer is measured at the center of the ball bond interface, and is shown in Fig 9. The sample size is no less than 5 for each test group. The average IMC layer thickness plus/minus standard deviation is 0.7 µm, 2.0 ± 0.6 µm, and 3.2 ± 0.2 µm, respectively. The IMC thickness is shown in Fig. 10 for various square root of aging time together with a control plot of Au-Al IMC [12]. The correlation coefficient of the linear fit is 0.998, which indicates that the IMC growth rate follows a parabolic relationship [3]:

$$x = kt^{1/2} \quad (2)$$

where x is the thickness of the IMC layer, k is the growth rate constant, and t is the aging time.The growth rate constant k is 0.10 ± 0.02 µm/h$^{1/2}$, and 1.64 µm/h$^{1/2}$ for PCS-Al, and Au-Al IMC layer, respectively.

The IMC layer forms mainly in the center of the ball bond interface. The width of the IMC layer in the cross-sectional plane remains almost unchanged from 96 h to 1344 h aging, and is 16.0-19.3 µm at 96 h and 17.2-22.7 µm at 1344 h. The horizontal IMC growth at PCS-Al interface is small compared with that of Au-Al interface, where the IMC width grows from 38 µm at 12 h to 47.8 µm at 200 h of aging at 175 °C [13].

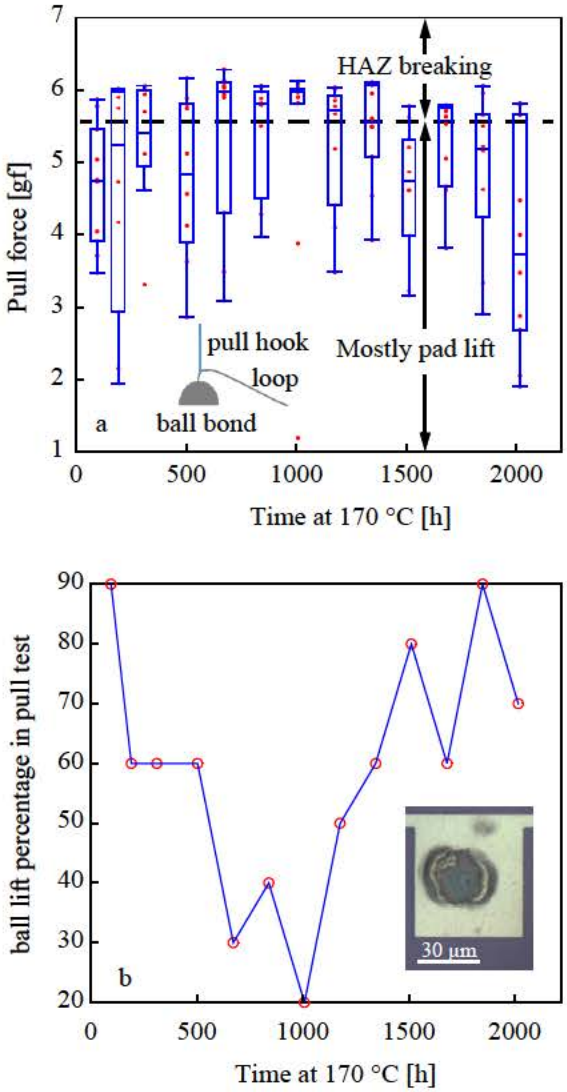

Figure 6. (a) Pull force, and (b) pad lift percentage in pull test from 96 h to 2016 h aging in 170 °C. Inset of (a) shows position of hook during pull test. Inset of (b) shows a typical pad lift fractography on pad side, example shown at 1848 h of aging.

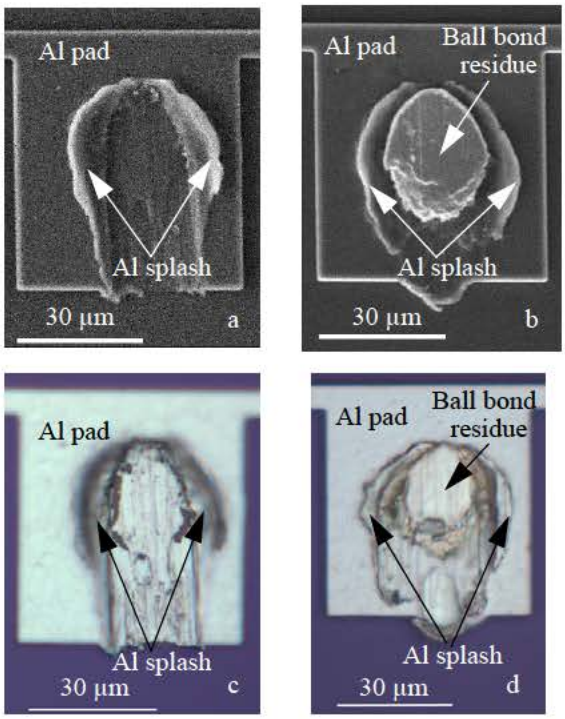

Figure 7. Typical chip side fractographies after ball bond shear test. SEM images of (a) through pad at 96 h, (b) through ball at 504 h, optical microscopic images of (c) through pad at 96 h, and (d) through ball at 168 h. (a) and (c) are taken from same sample. SEM images are taken with secondary electron signals.

International Symposium on Microelectronics: FALL 2015, Vol. 2015, No. 1, pp. 000298-000304
http://www.imapsource.org/doi/abs/10.4071/isom-2015-WA53
http://dx.doi.org/10.4071/isom-2015-WA53
Authors' Postprint:

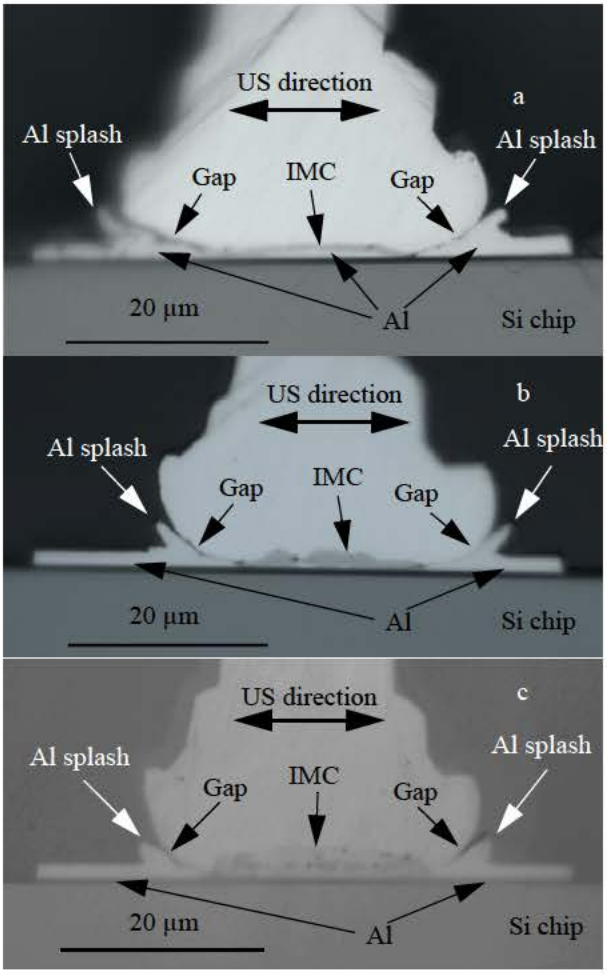

Figure 8. Optical microscopic images of cross-sections of PCS ball bonds aged at 170 °C for (a) 96 h, (b) 504 h, and (c) 1344 h, respectively.

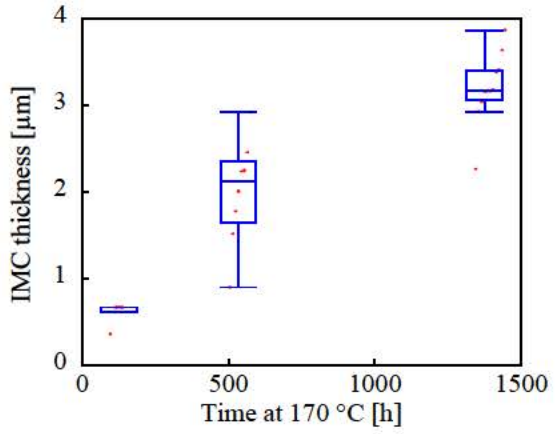

Figure 9. IMC thickness at center of ball bond interface of samples aged at 170 °C for 96 h, 504 h, and 1344 h, respectively.

3.3 SEM and EDX study on cross-sections

The SEM cross-sectional image of a typical ball bond aged for 1344 h is shown in Fig. 11. EDX results are given for locations A and B in Fig. 11. More detailed images of the same sample are shown in Figs. 12a-c. The composition of point D in Fig. 12a is studied with EDX and shown in Table 2.

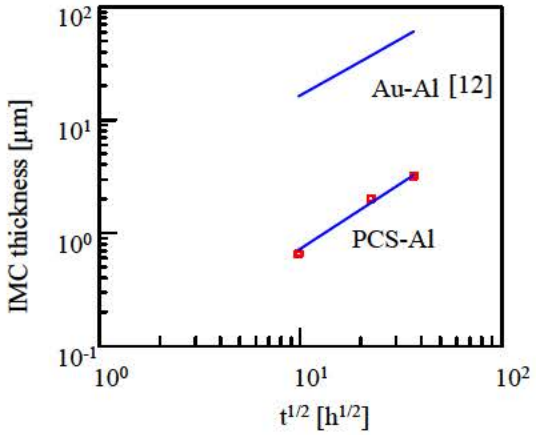

Figure 10. IMC thickness vs. square root of aging time *t* at 170 °C for Au-Al [12] and PCS-Al, respectively.

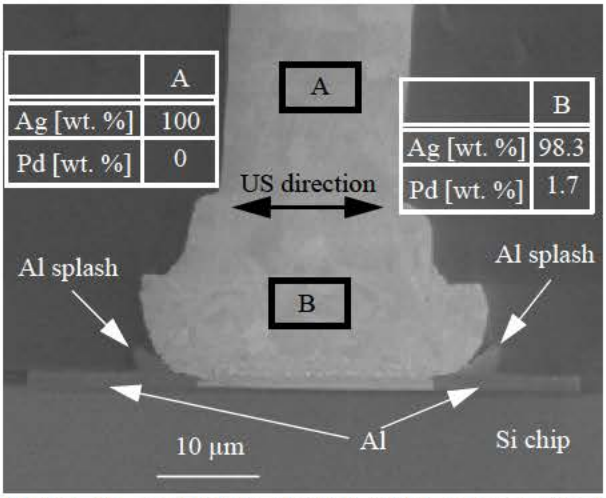

Figure 11. Secondary electron SEM cross-sectional image of PCS ball bonds aged at 170 °C for 1344 h.

Table 2: Compositions of point D in Fig. 12

	wt. %	at. %
Al	6.0	20.4
Pd	1.2	1.0
Ag	92.8	78.6

International Symposium on Microelectronics: FALL 2015, Vol. 2015, No. 1, pp. 000298-000304
http://www.imapsource.org/doi/abs/10.4071/isom-2015-WA53
http://dx.doi.org/10.4071/isom-2015-WA53
Authors' Postprint:

4. Discussion

4.1 IMC composition

According to the Ag-Al binary phase diagram, three IMCs can form and two IMCs can exist at below 300 °C, namely the μ- and δ-phases. The compositions of the μ- and δ-phases are 21-25 at.% Al and 33-41 at.% Al, respectively at 200 °C [14]. Generally the wider composition range of an IMC indicates less brittleness. The composition ranges of the μ- and δ-phases are 4 at.% and 8 at.%, respectively, which are both much wider than any Au-Al IMCs, where the widest composition range is only 1 at.%. According to [1] however, the μ-phase forms at 250-450 °C. Therefore the main IMC that can form at the interface between a Ag ball bond and an Al pad at 170 °C is expected to be the δ-phase.

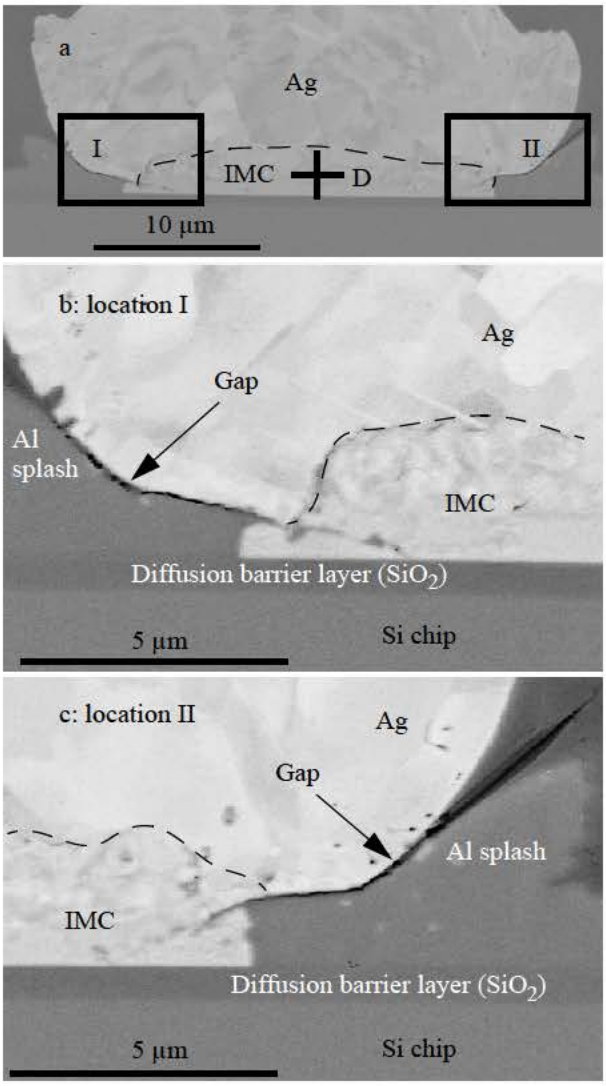

Figure 12. SEM images of (a) overview at 3k× magnification, (b) location I, and (c) location II at 10k× magnification, respectively, of cross-section of typical ball bond interface.

4.2 Volume change due to IMC formation

The volume change associated with the formation of the δ-phase is +1.3 % [1], resulting in compressive stress inside the IMC layer, in contrast to the situation of a Au wire bond where two IMCs can form initially at the interface between a Au ball bond and an Al pad, namely Au_8Al_3 and Au_2Al [3, 15]. The formation of Au_8Al_3 and Au_2Al results in volume change of -2.3 % and -5.7 %, respectively [16], leading to tensile stress inside the IMC layer. [17-21]

5. Conclusions

Thermal aging behavior is studied for fine pitch ball bond made with Pd coated Ag on Al metallization with shear test, pull test, and cross-sectioning. The shear strength and pull force remains high for up to 2016 h of aging at 170 °C. Cross-sectioning has revealed the evolution of the IMC layer at the ball bond interface. Compared with data available for Au, the IMC thickness grows significantly slower with Ag than with Au, which indicates longer survival in a high temperature environment. Therefore, Pd coated Ag wire is potentially a new alternative to Au wire in the wire bonding industry.

Acknowledgments

This work is supported by the Canadian Natural Science and Engineering Research Council (NSERC), and the Initiative for Automotive Manufacturing Innovation (IAMI), Ontario.

References

[1] Guo, Rui, Tao Hang, Dali Mao, Ming Li, Kaiyou Qian, Zhong Lv, and Hope Chiu. "Behavior of intermetallics formation and evolution in Ag–8Au–3Pd alloy wire bonds." Journal of Alloys and Compounds 588 (2014): 622-627.

[2] Cho, Jong-Soo, Hee-Suk Jeong, Jeong-Tak Moon, Se-Jin Yoo, Jae-Seok Seo, Seung-Mi Lee, Seung-Weon Ha, Eun-Kyu Her, Suk-Hoon Kang, and Kyu-Hwan Oh. "Thermal reliability & IMC behavior of low cost alternative Au-Ag-Pd wire bonds to Al metallization." In Electronic Components and Technology Conference, 2009. ECTC 2009. 59th, pp. 1569-1573. IEEE, 2009.

[3] Harman, George G. Wire bonding in microelectronics. McGraw-Hill, 2010.

[4] Cho, Jong-Soo, Kyeong-Ah Yoo, Sung-Jae Hong, Jeong-Tak Moon, Yong-Je Lee, Wongil Han, Hanki Park et al. "Pd effects on the reliability in the low cost Ag bonding wire." In Electronic Components and Technology Conference (ECTC), 2010 Proceedings 60th, pp. 1541-1546. IEEE, 2010.

International Symposium on Microelectronics: FALL 2015, Vol. 2015, No. 1, pp. 000298-000304
http://www.imapsource.org/doi/abs/10.4071/isom-2015-WA53
http://dx.doi.org/10.4071/isom-2015-WA53
Authors' Postprint:

[5] Tseng, Yi-Wei, Fei-Yi Hung, Truan-Sheng Lui, Mei-Yu Chen, and Hao-Wen Hsueh. "Effect of annealing on the microstructure and bonding interface properties of Ag–2Pd alloy wire." Microelectronics Reliability (2015).

[6] Jiaqing Xi, Norbe Mendoza, Kevin Chen, Thomas Yang, Edward Reyes, Steve Bezuk. "Evaluation of Ag Wire Reliability on Fine Pitch Wire Bonding." In Electronic Components and Technology Conference (ECTC), 2015 Proceedings 65th, pp. 1392-1395. IEEE, 2015.

[7] Tanna, Suresh, Jairus L. Pisigan, W. H. Song, Christopher Halmo, John Persic, and Michael Mayer. "Low cost Pd coated Ag bonding wire for high quality FAB in air." In Electronic Components and Technology Conference (ECTC), 2012 IEEE 62nd, pp. 1103-1109. IEEE, 2012.

[8] Ly, Nhat, Di Erick Xu, Wan Ho Song, and Michael Mayer. "More uniform Pd distribution in free-air balls of Pd-coated Cu bonding wire using movable flame-off electrode." Microelectronics Reliability 55, no. 1 (2015): 201-206.

[9] Uno, Tomohiro, Shinichi Terashima, and Takashi Yamada. "Surface-enhanced copper bonding wire for LSI." In Electronic Components and Technology Conference, 2009. ECTC 2009. 59th, pp. 1486-1495. IEEE, 2009.

[10] Gomes, J., M. Mayer, and B. Lin. "Development of a fast method for optimization of Au ball bond process." Microelectronics Reliability (2015).

[11] Hui Xu, Alireza Rezvani, Jon Brunner, John Foley, Ivy Qin, and Bob Chylak. "Development of Advanced Wire Bonding Technology for QFN Devices." In Electronic Components and Technology Conference (ECTC), 2015 Proceedings 65th, pp. 1385-1391. IEEE, 2015.

[12] Philofsky, Elliott. "Intermetallic formation in gold-aluminum systems." Solid-State Electronics 13, no. 10 (1970): 1391-1394.

[13] Breach, C. D., and F. Wulff. "New observations on intermetallic compound formation in gold ball bonds: general growth patterns and identification of two forms of Au 4 Al." Microelectronics Reliability 44, no. 6 (2004): 973-981.

[14] McAlister, A. J. "The Ag− Al (Silver-Aluminum) system." Bulletin of Alloy Phase Diagrams 8, no. 6 (1987): 526-533.

[15] Xu, Hui, Changqing Liu, Vadim V. Silberschmidt, S. S. Pramana, Timothy John White, Zhong Chen, M. Sivakumar, and V. L. Acoff. "A micromechanism study of thermosonic gold wire bonding on aluminum pad." Journal of applied physics 108, no. 11 (2010): 113517.

[16] Xu, H., C. Liu, V. V. Silberschmidt, S. S. Pramana, T. J. White, Z. Chen, and V. L. Acoff. "New mechanisms of void growth in Au–Al wire bonds: volumetric shrinkage and intermetallic oxidation." Scripta Materialia 65, no. 7 (2011): 642-645.

[17] McCracken, Michael James, Yasumasa Koda, Hyoung Joon Kim, Michael Mayer, John Persic, June Sub Hwang, and Jeong-Tak Moon. "Explaining Nondestructive Bond Stress Data From High-Temperature Testing of Au-Al Wire Bonds." Components, Packaging and Manufacturing Technology, IEEE Transactions on 3, no. 12 (2013): 2029-2036.

[18] Mayer, M. "Non-destructive monitoring of Au ball bond stress during high-temperature aging." In Electronic Components and Technology Conference, 2008. ECTC 2008. 58th, pp. 1762-1768. IEEE, 2008.

[19] Mayer, M., J. T. Moon, and J. Persic. "Measuring stress next to Au ball bond during high temperature aging." Microelectronics Reliability 49, no. 7 (2009): 771-781.

[20] McCracken, Michael J., Hyoung Joon Kim, Michael Mayer, John Persic, June Sub Hwang, and Jeong-Tak Moon. "Assessing Au-Al wire bond reliability using integrated stress sensors." In Thermal and Thermomechanical Phenomena in Electronic Systems (ITherm), 2010 12th IEEE Intersociety Conference on, pp. 1-9. IEEE, 2010.

[21] Gomes, J., and M. Mayer. "Effect of Au ball bond geometry on bond strength and process parameters, and assessing reliability on Al bond pad using integrated stress sensors." In Electronic Components and Technology Conference (ECTC), 2015 IEEE 65th, pp. 2127-2133. IEEE, 2015.